Proceedings of DSCC 2015
ASME 2015 Dynamic Systems and Control Conference
October 28-30, 2015, Columbus, Ohio, USA

DSCC2015-9943

HYBRID SYSTEM BASED ANALYTICAL APPROACH FOR OPTIMAL GEAR SHIFTING SCHEDULE DESIGN

Chaozhe R. He *
Department of Mechanical Engineering
University of Michigan
Ann Arbor, Michigan 48109
Email: hchaozhe@umich.edu

Wubing B. Qin
Department of Mechanical Engineering
University of Michigan
Ann Arbor, Michigan 48109
Email: wubing@umich.edu

Necmiye Ozay
Department of Electrical Engineering
and Computer Science
University of Michigan
Ann Arbor, Michigan 48109
Email: necmiye@umich.edu

Gábor Orosz
Department of Mechanical Engineering
University of Michigan
Ann Arbor, Michigan 48109
Email: orosz@umich.edu

ABSTRACT

In this paper, we present a systematic design for gear shifting using a hybrid system approach. The longitudinal motion of the vehicle is regulated by a PI-controller that determines the required axle torque. The gear scheduling problem is modeled as a hybrid system and an optimization-based gear shifting strategy is introduced, which guarantees that the propulsion requirements are delivered while minimizing fuel consumption. The resulting dynamics is proved to be stable theoretically. In a case study, we compare our strategy with a standard approach used in the industry and demonstrate the advantages of our design for class 8 trucks.

1 INTRODUCTION

Most vehicles driven on US roads are equipped with automated transmission and designing the gear shift schedule appropriately allows one to improve the fuel economy of road vehicles. Gear schedule design usually considers driver command (pedal/throttle position) and vehicle states (usually speed) to determine when to shift gears. A popular method of gear shift design used in the industry is to identify curve on the plane of engine speed and pedal position where the engine gives the best fuel economy and then design the up and down shifts so that the engine states stay close to this curve [1,2,3]. In [4], a dynamic 3-state-based (vehicle speed, pedal position, and acceleration) neural network model was proposed and proven to outperform a traditional shift logic. In [5], knowledge from experienced drivers were used for designing gear shift logic for automated manual transmission, to achieve the performance of experienced driver with a manual transmission. In [6], rule-based shift logic was designed using a fuzzy neural network approach. In [7], two gear shift schedules were proposed, one to obtain the best performance and the other to obtain best fuel economy. Based on these two maps, the gear shift schedule for dual clutch transmission was proposed in [8], based on fuzzy logic.

In all the designs mentioned above, the gear shift curves are converted to the plane of longitudinal velocity and pedal position as shown in Fig. 1(a). The performance is often compromised due to the lack of knowledge on varying environment or misinterpretation of drivers' intention, as the torque demand may

*Address all correspondence to this author.

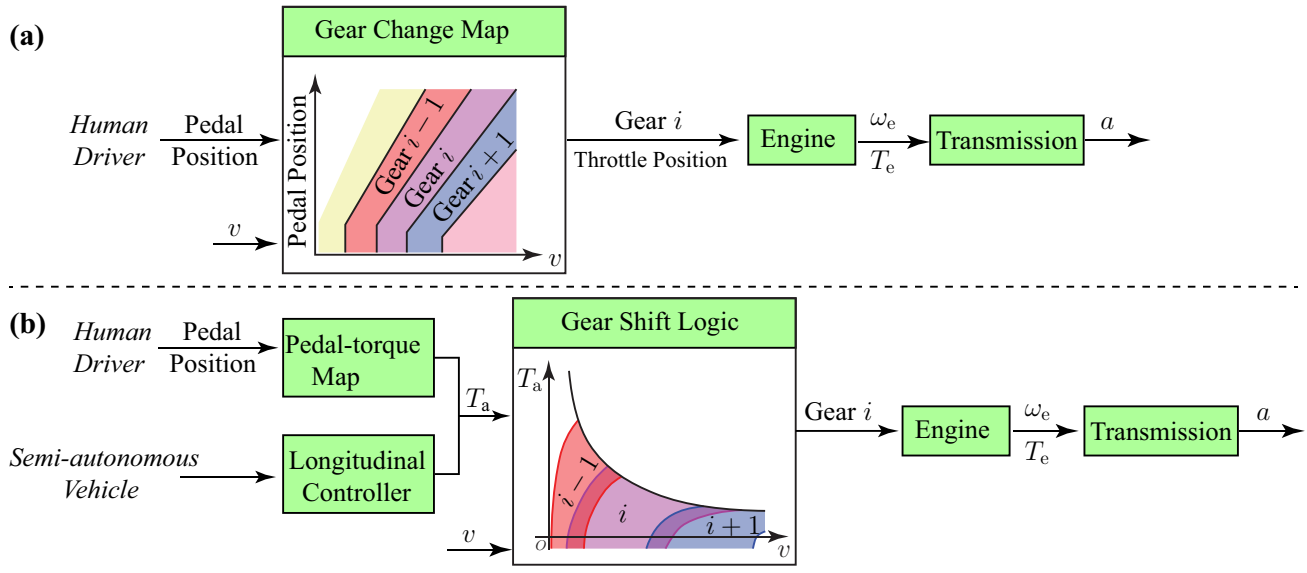

Figure 1: Design concepts for gear shift schedule. T_a is the axle torque required, v is the speed of the vehicle, T_e is the engine torque, ω_e is the engine speed, and a is the acceleration of the vehicle.

depend nonlinearly on the pedal position.

On the other hand, vehicles of increased level of autonomy and connectivity are becoming available due to their potential for improving safety, mobility, and fuel economy. In particular, for the longitudinal dynamics, features like adaptive cruise control (ACC) are available in many cars and advanced concepts like connected cruise control (CCC) are heavily researched in academia and industry [9]. These controllers demand axle torque that can be ensured by setting the engine torque and the gears appropriately while bypassing the need for monitoring pedal position. This requires a new design framework which allows the vehicle to function in semi-autonomous mode as well as in human-driven mode while maintaining good fuel efficiency in both cases.

In this paper we consider the framework proposed in Fig. 1(b) to design an optimal gear shift strategy.

The gear shift logic design now is done using a first principle dynamic model and direct optimization, and it guarantees the torque demand is achieved in the most fuel efficient way. This design is superior to the traditional design in terms of fuel economy as will be demonstrated below. We remark that in human-driven mode one may still include a pedal position vs. torque map that depends on the "driving style" of the driver.

The dynamics of a semi-autonomous or human driven vehicle with automated transmission can be modeled as a hybrid system which contains dynamic variables of both discrete and continuous types [10,11,12]. Proving stability for these systems is challenging especially when the governing equations are nonlinear [13–16], that is certainly the case for automobiles. In this paper we take a hybrid system approach to analyze the dynamics subject to our gear shift design. Specifically, we use this approach to provide a systematic method that ensures the stability of different operating points. In order to make the problem analytically tractable, the longitudinal motion of the vehicle is modeled by differential equations, the fuel consumption of the engine is calculated using a static map, and the gear shifts are considered to be instantaneous.

The remainder of the paper is organized as follows. In Sections 2 we describe the modeling framework that leads to a hybrid system. Then we present the switching logic in Section 3 and prove that it can be used to achieve stable operating points in Section 4. In Section 5 we demonstrate that our design can outperform the traditional design and conclusions are drawn in Section 6.

2 VEHICLE DYNAMICS WITH GEAR CHANGES

In this section we describe the longitudinal dynamics of the vehicle using differential equations and analyze the stability of equilibria. Then we rewrite the equations using engine-based quantities to include the gear change explicitly.

2.1 Modeling Vehicle Dynamics

Here we use the longitudinal vehicle model from [17,18]. Neglecting the flexibility of the suspension and the tires, using

power law one may obtain

$$m_{\text{eff}}\dot{v} = -mg\sin\phi - \gamma_0 mg\cos\phi - k_0(v+v_{\text{w}})^2 + \frac{\eta}{R}T_{\text{e}}, \qquad (1)$$

where $m_{\text{eff}} = m + J/R^2$ is the effective mass, containing the mass of vehicle m, the mass moment of inertia J of the rotating elements, and the wheel radius R. Also, g is the gravitational constant, ϕ is the inclination angle, γ_0 is the rolling resistance coefficient, k_0 is the air drag constant, v_{w} is the velocity of the head wind, η is the gear ratio. Finally, T_{e} is the engine torque, which is the control input that we need to design. For simplicity, we assume the vehicle is traveling on a flat road without headwind, i.e., $\phi = 0$ and $v_{\text{w}} = 0$, yielding

$$\dot{v} = -\gamma g - k v^2 + a_{\text{d}}, \qquad (2)$$

where

$$\gamma = \frac{m}{m_{\text{eff}}}\gamma_0, \qquad k = \frac{k_0}{m_{\text{eff}}}, \qquad a_{\text{d}} = \frac{\eta}{m_{\text{eff}}R}T_{\text{e}}. \qquad (3)$$

Here a_{d} is a re-scaled torque with unit [m/s^2].

In order to maintain a reference velocity v_{r}, we use the PI controller

$$\begin{aligned} a_{\text{d}} &= K_{\text{P}}\dot{e} + K_{\text{I}}e, \\ \dot{e} &= v_{\text{r}} - v. \end{aligned} \qquad (4)$$

Thus, (2,4) give the closed-loop vehicle dynamics

$$\begin{cases} \dot{v} = -\gamma g - k v^2 + K_{\text{P}}\big(v_{\text{r}} - v\big) + K_{\text{I}}e, \\ \dot{e} = v_{\text{r}} - v. \end{cases} \qquad (5)$$

To analyze the power consumption, we rewrite (5) in terms of the variables v and a_{d}, that is,

$$\begin{cases} \dot{v} \;\; = -\gamma g - k v^2 + a_{\text{d}}, \\ \dot{a}_{\text{d}} = K_{\text{P}}\gamma g - K_{\text{I}}v + K_{\text{P}}k v^2 - K_{\text{P}}a_{\text{d}} + K_{\text{I}}v_{\text{r}} + K_{\text{P}}\dot{v}_{\text{r}}. \end{cases} \qquad (6)$$

When considering constant reference speed $v_{\text{r}}(t) \equiv v_{\text{r}}^*$, system (6) possesses the equilibrium

$$\begin{cases} v^* = v_{\text{r}}^*, \\ a_{\text{d}}^* = \gamma g + k(v_{\text{r}}^*)^2. \end{cases} \qquad (7)$$

Defining the perturbations

$$\begin{cases} \tilde{v} = v - v^*, \\ \tilde{a}_{\text{d}} = a_{\text{d}} - a_{\text{d}}^*, \end{cases} \qquad (8)$$

(6) can be re-written as

$$\begin{cases} \dot{\tilde{v}} \;\; = -2k v^*\tilde{v} + \tilde{a}_{\text{d}} - k\tilde{v}^2, \\ \dot{\tilde{a}}_{\text{d}} = (2K_{\text{P}}k v^* - K_{\text{I}})\tilde{v} - K_{\text{P}}\tilde{a}_{\text{d}} + K_{\text{P}}k\tilde{v}^2. \end{cases} \qquad (9)$$

Then we can state the following lemma about stability.

Lemma 1. *The trivial equilibrium of the dynamic system* (9) *is asymptotically stable if* $\tilde{v} > -K_{\text{P}}/k - 2v^*$.

Proof. Choosing the Lyapunov function

$$V(\tilde{v},\tilde{a}_{\text{d}}) = \frac{1}{2}A\tilde{v}^2 + \frac{1}{2}B(\tilde{a}_{\text{d}} + K_{\text{P}}\tilde{v})^2, \qquad (10)$$

with $A > 0, B > 0$, we obtain the Lie derivative

$$\dot{V}(\tilde{v},\tilde{a}_{\text{d}}) = -A\left(k\tilde{v} + 2kv^* + \frac{BK_{\text{I}}K_{\text{P}}}{A}\right)\tilde{v}^2 + (A - BK_{\text{I}})\tilde{v}\tilde{a}_{\text{d}}. \qquad (11)$$

If we select $A = BK_{\text{I}}$, then (11) is negative semi-definite when $\tilde{v} > K_{\text{P}}/k - 2v^*$. Applying the LaSalle-Krasovskii invariance principle, it can be shown that the largest invariant set within $\dot{V} = 0$ is $(\tilde{v},\, \tilde{a}_{\text{d}}) = (0,0)$. Therefore, the trivial equilibrium of the dynamic system (9) is asymptotically stable with the region of attraction being $\{(\tilde{v},\tilde{a}_{\text{d}}) | \tilde{v} > -K_{\text{P}}/k - 2v^*\}$. □

Note that since $-K_{\text{P}}/k - 2v^*$ is negative for $v^* > 0$, setting large enough K_{p} allows us to make the region of attraction, bounded by a contour of the Lyapunov function (10), large enough so that it covers the operating region of the vehicle.

2.2 Introducing Gear Change

Assume that the transmission system has N gears, i.e., $\eta \in \{\eta_i \,|\, i \in \{1,2,\cdots,N\}\}$. Then with ith gear applied, the angular speed of the engine and the engine torque are given by

$$\omega_{\text{e}} = \frac{\eta_i}{R}v, \quad T_{\text{e}} = \frac{m_{\text{eff}}R}{\eta_i}a_{\text{d}}, \qquad (12)$$

that defines a linear transformation from (v, a_{d})-space to (ω, T_{e})-space. Henceforth, the closed-loop dynamics (6) can be rewritten

as

$$\begin{cases} \dot{\omega}_\mathrm{e} = -\dfrac{\eta_i}{R}\gamma \mathrm{g} - k\dfrac{R}{\eta_i}\omega_\mathrm{e}^2 + \dfrac{\eta_i^2}{m_\mathrm{eff}R^2}T_\mathrm{e}, \\ \dot{T}_\mathrm{e} = \dfrac{m_\mathrm{eff}R}{\eta_i}K_\mathrm{P}\gamma \mathrm{g} - \dfrac{m_\mathrm{eff}R^2}{\eta_i^2}K_\mathrm{I}\omega_\mathrm{e} + \dfrac{m_\mathrm{eff}R^3}{\eta_i^3}K_\mathrm{P}k\omega_\mathrm{e}^2 - K_\mathrm{P}T_\mathrm{e} \\ \qquad + \dfrac{m_\mathrm{eff}R}{\eta_i}K_\mathrm{I}v_\mathrm{r} + \dfrac{m_\mathrm{eff}R}{\eta_i}K_\mathrm{P}\dot{v}_\mathrm{r}. \end{cases} \tag{13}$$

Defining the state as $x = [\omega_\mathrm{e}, T_\mathrm{e}]^\mathrm{T}$ and the input as $u = v_\mathrm{r}$, the dynamics (13) with gear change can be written into the compact form

$$\begin{array}{ll} \dot{x}(t) = f_i\big(x(t),u(t)\big), & \text{if} \quad x \in \mathscr{X}_i \subseteq \mathbb{R}^2, \\ i(k+1) = z_i(x(t),i(k)), & \text{if} \quad x \in \partial\mathscr{X}_i, \end{array} \tag{14}$$

where $i \in \{1,\cdots,N\}$ and $k = 1,2,\ldots$ is the event number for gear shift. The function f_i, represents the right hand side of (13) and it describes the dynamics of each continuous-time subsystem for each gear i when the state evolves inside the set $\mathscr{X}_i$. Moreover, z_i represents the gear shift schedule to be designed and describes the switches at the boundary of the set $\mathscr{X}_i$ (denoted by $\partial\mathscr{X}_i$). We want to design the gear switch logic to achieve optimal fuel consumption while still guaranteeing the stability of the overall hybrid system (14). For a fixed gear ratio, stability can be guaranteed by the following lemma:

Lemma 2. *With a fixed gear the stability of the vehicle dynamics* (5) *is equivalent to the engine dynamics* (14)*.*

Proof. This holds since the linear transformation (12) does not affect stability.□

We remark that in Lemma 1 and 2 we did not consider engine saturation (explained in detail in the next section) but we still assume that the controller ensures stability of the equilibrium. The proof of this statement is left for future research.

3 GEAR SWITCHING STRATEGY

In this section we introduce the mathematical tools we need for the gear shift schedule design and then we explain the details of the design process. The goal here is to design a switching schedule that minimizes the fuel consumption.

The fuel consumption can be quantified by measuring the mass flow rate of fuel $\dot{m}_\mathrm{f} = q(\omega_\mathrm{e}, T_\mathrm{e})$ as a function of the engine speed ω_e and engine torque T_e. To determine how efficiently the engine uses fuel while producing power $P = \omega_\mathrm{e}T_\mathrm{e}$, one can use the brake specific fuel consumption (BSFC) defined by

$$\mathrm{BSFC} = g(\omega_\mathrm{e}, T_\mathrm{e}) = \frac{\dot{m}_\mathrm{f}}{P} = \frac{q(\omega_\mathrm{e}, T_\mathrm{e})}{\omega_\mathrm{e}T_\mathrm{e}}, \tag{15}$$

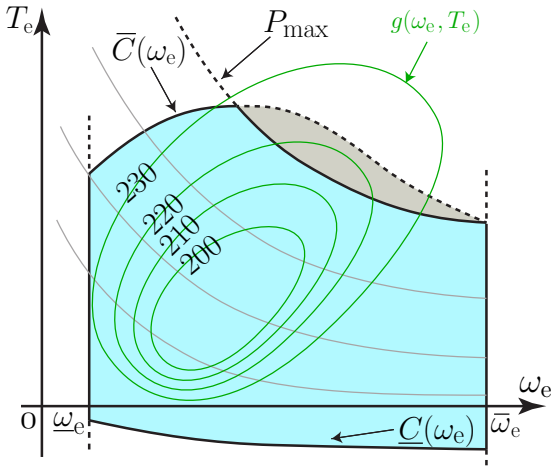

Figure 2: Conceptual BSFC diagram. The green contours correspond to the constant levels of BSFC $g(\omega_\mathrm{e}, T_\mathrm{e}) = c$, the grey curves represent the iso-power curves and the black curves represent the limitation of the engine. Since the grey region is only accessible in certain gears, the blue region is considered as the engine operating region.

see [19]. In practice, the function $g(\omega_\mathrm{e}, T_\mathrm{e})$ is nonlinear and does not have an analytical expression, but it may be attainted experimentally and one may use interpolation to obtain the value of g for $(\omega_\mathrm{e}, T_\mathrm{e})$ combinations where measurements are not available. Typically $g(\omega_\mathrm{e}, T_\mathrm{e})$ has one minimum point, at which the engine gives the best fuel economy. In Fig. 2, the contours of a conceptual BSFC function are plotted as green curves, together with the maximum and minimum constraints on the engine torque and engine speed, i.e., $\underline{C}(\omega_\mathrm{e}) \le T_\mathrm{e} \le \overline{C}(\omega_\mathrm{e})$ and $\underline{\omega}_\mathrm{e} \le \omega_\mathrm{e} \le \overline{\omega}_\mathrm{e}$. Note that the grey region is only accessible in certain gears (i.e., gear change would lead to a working point where the engine limitation is exceeded) and it is typically very small in practice. Thus, to simplify the derivation, we use the iso-power curve P_max to bound the blue operating region that is given by

$$\omega_\mathrm{e} \in [\underline{\omega}_\mathrm{e}, \overline{\omega}_\mathrm{e}], \quad T_\mathrm{e} \in [\underline{C}(\omega_\mathrm{e}), \overline{C}(\omega_\mathrm{e})], \quad T_\mathrm{e}\omega_\mathrm{e} \le P_\mathrm{max}. \tag{16}$$

Also note that an engine can output negative torque, but the maximum absolute value of the negative torque is much smaller than that of the positive torque. Moreover, fuel consumption measurements are typically available for positive torque values only. Thus, we assume that the fuel consumption is zero along the curve $\underline{C}(\omega_\mathrm{e})$ corresponding to the minimum available torque and use interpolation to quantify the fuel consumption for zero and negative torque values. Still, for $T_\mathrm{e} \le 0$ we use the strategy designed for small $T_\mathrm{e} > 0$ in order to avoid difficulties due to singularity of the BSFC.

We assume that the gear ratio is monotonically decreasing

and no gear skipping is possible, that is,

$$\begin{aligned} &\eta_1 > \eta_2 > \cdots > \eta_N \\ &i(k+1) \in \{i(k)-1, i(k)+1\}, \end{aligned} \tag{17}$$

for $i \in \{1,\cdots,N\}$ and $k = 1,2,\ldots$ We also assume that shifting happens instantaneously along the iso-power curves shown as light grey curves in Fig. 2. Mathematically, such gear shift process is described as

$$m_{\text{eff}} a_{\text{d}} v = T_{\text{e}}^{(i)} \omega_{\text{e}}^{(i)}, \quad \frac{\omega_{\text{e}}^{(i)}}{\eta_i} = \frac{\omega_{\text{e}}^{(i+1)}}{\eta_{i+1}}, \quad T_{\text{e}}^{(i)} \eta_i = T_{\text{e}}^{(i+1)} \eta_{i+1}, \tag{18}$$

for $i \in \{1,\cdots,N\}$.

Our gear change strategy is to choose the gear with smallest BSFC value, which is shown graphically in Fig. 3. The green contours correspond to $g\big(\omega_{\text{e}}^{(i)}, T_{\text{e}}^{(i)}\big) = c$, the purple contours correspond to $g\big(\frac{\omega_{\text{e}}^{(i)}\eta_{i+1}}{\eta_i}, \frac{T_{\text{e}}^{(i)}\eta_i}{\eta_{i+1}}\big) = c$, while the pink contours correspond to $g\big(\frac{\omega_{\text{e}}^{(i)}\eta_{i-1}}{\eta_i}, \frac{T_{\text{e}}^{(i)}\eta_i}{\eta_{i-1}}\big) = c$. The upshift curve $h_i^+(\omega_{\text{e}})$, is determined by

$$g\big(\omega_{\text{e}}^{(i)}, h_i^+(\omega_{\text{e}}^{(i)})\big) = g\left(\frac{\omega_{\text{e}}^{(i)}\eta_{i+1}}{\eta_i}, \frac{h_i^+(\omega_{\text{e}}^{(i)})\eta_i}{\eta_{i+1}}\right), \tag{19}$$

that is visualized in Fig. 3 by the blue curves obtained from intersections of green and purple contours (denoted by blue dots). To be able to solve (19) for the function $h_i^+(\omega_{\text{e}})$, the conditions for implicit function theorem are assumed to hold. Crossing this curve to the right, i.e., shifting one gear up will give a smaller BSFC value. Note that we need to satisfy the engine speed constraint, $\omega_{\text{e}}^{(i+1)} \geq \underline{\omega}_{\text{e}}$ corresponding to the right black vertical line at the bottom of Fig. 3. The upshift boundary that combines this constraint with $h_i^+(\omega_{\text{e}})$ is denoted by $H_i^+(\omega_{\text{e}}, T_{\text{e}}) = 0$.

Similarly, the downshift curve $h_i^-(\omega_{\text{e}})$, is given by

$$g\big(\omega_{\text{e}}^{(i)}, h_i^-(\omega_{\text{e}}^{(i)})\big) = g\left(\frac{\omega_{\text{e}}^{(i)}\eta_{i-1}}{\eta_i}, \frac{h_i^-(\omega_{\text{e}}^{(i)})\eta_i}{\eta_{i-1}}\right), \tag{20}$$

and it is also visualized in Fig. 3. Again, the conditions for implicit function theorem are assumed to hold. Crossing this curve to the left, i.e., shifting one gear down will give a smaller BSFC value. Moreover, we need to satisfy the engine speed constraint $\omega_{\text{e}}^{(i)} \geq \underline{\omega}_{\text{e}}$ (see left black vertical line in Fig. 3). We denote the downshift boundary that combines speed constraint with $h_i^-(\omega_{\text{e}})$ by $H_i^-(\omega_{\text{e}}, T_{\text{e}}) = 0$.

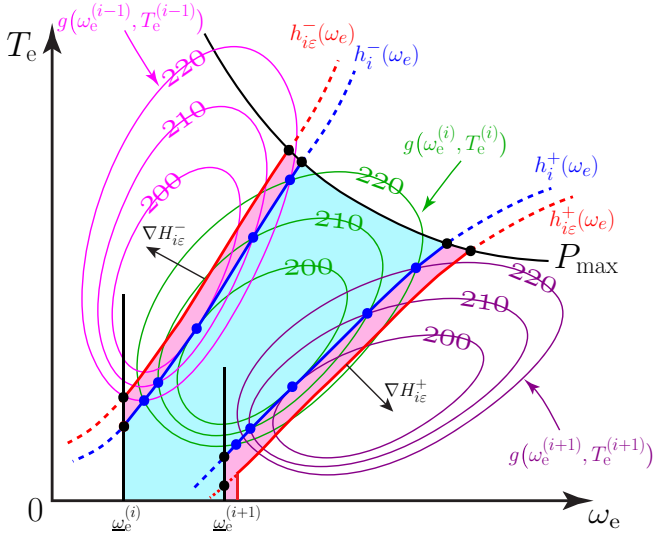

Figure 3: Gear shift concept. The magenta contours, green contours and purple contours represent the BSFC level sets as functions of the engine speed ω_{e} and torque T_{e} at the $(i-1)$-th, i-th and $(i+1)$-th gear respectively. The vertical black lines at the bottom represent the minimum engine speed at i-th and $(i+1)$-th gear respectively, while the black curve on the top corresponds to the maximum power. The union of the blue and the red shaded regions is the actual working region for the i-th gear $\mathscr{X}_i$.

To avoid ambiguity when the working point is on the curve $h_i^+(\omega_{\text{e}})$ or $h_i^-(\omega_{\text{e}})$, we introduce hysteresis by defining the ε-tolerance curves $h_{i\varepsilon}^+(\omega_{\text{e}})$ and $h_{i\varepsilon}^-(\omega_{\text{e}})$, that can be obtained by relaxing (19) and (20) to

$$g\big(\omega_{\text{e}}^{(i)}, h_{i\varepsilon}^+(\omega_{\text{e}}^{(i)})\big) = g\left(\frac{\omega_{\text{e}}^{(i)}\eta_{i+1}}{\eta_i}, \frac{h_{i\varepsilon}^+(\omega_{\text{e}}^{(i)})\eta_i}{\eta_{i+1}}\right)(1+\varepsilon), \tag{21}$$

$$g\big(\omega_{\text{e}}^{(i)}, h_{i\varepsilon}^-(\omega_{\text{e}}^{(i)})\big) = g\left(\frac{\omega_{\text{e}}^{(i)}\eta_{i-1}}{\eta_i}, \frac{h_{i\varepsilon}^-(\omega_{\text{e}}^{(i)})\eta_i}{\eta_{i-1}}\right)(1+\varepsilon), \tag{22}$$

as shown by the red curves in Fig. 3. Similar to $H_i^+(\omega_{\text{e}}, T_{\text{e}}) = 0$ and $H_i^-(\omega_{\text{e}}, T_{\text{e}}) = 0$, we can define $H_{i\varepsilon}^+(\omega_{\text{e}}, T_{\text{e}}) = 0$ and $H_{i\varepsilon}^-(\omega_{\text{e}}, T_{\text{e}}) = 0$, which include $h_{i\varepsilon}^+(\omega_{\text{e}})$ and $h_{i\varepsilon}^-(\omega_{\text{e}})$, and the solid black vertical lines in Fig. 3. For the i-th gear, constraints $\omega_{\text{e}} T_{\text{e}} < P_{\max}, H_{i\varepsilon}^+(\omega_{\text{e}}, T_{\text{e}}) < 0, H_{i\varepsilon}^-(\omega_{\text{e}}, T_{\text{e}}) < 0$ define the working region $\mathscr{X}_i$ which is the union of the blue shaded region and the red shaded regions in Fig. 3. It should be noted that $\mathscr{X}_i$ may be different for each i.

Therefore, the gear shift schedule can be formally written as

$$\begin{aligned} &\text{if} \quad H^+_{i\varepsilon}(\omega_e(t^-), T_e(t^-)) = 0, \quad [\dot{\omega}_e, \dot{T}_e] \cdot \nabla H^+_{i\varepsilon}|_{t=t^-} > 0, \\ &\text{then} \quad i(t^+) = i(t^-) + 1, \\ &\text{if} \quad H^-_{i\varepsilon}(\omega_e(t^-), T_e(t^-)) = 0, \quad [\dot{\omega}_e, \dot{T}_e] \cdot \nabla H^-_{i\varepsilon}|_{t=t^-} > 0, \\ &\text{then} \quad i(t^+) = i(t^-) - 1, \end{aligned} \tag{23}$$

where ∇ is the nabla or gradient operator for multi-variable functions, as illustrated in Fig. 3.

4 STABILITY WITH GEAR CHANGES

In this section, we prove that the hybrid system (14) is stable in the sense of Lyapunov with the proposed gear shift schedule. Before stating the main result of the section, we present some useful definitions that are visualized graphically in Fig. 4.

Definition 1. *A partition of a compact set $\mathscr{X} \subseteq \mathbb{R}^2$ is a collection of subsets $\{P_i\}_{i=1}^k$, $P_i \subseteq \mathscr{X}, P_i \neq \emptyset$, such that $\bigcup_{i=1}^k P_i = \mathscr{X}$ and $P_i \bigcap P_j = \emptyset, \forall i \neq j$.*

As shown in Fig. 4(a), the partition means that the P_i-s cover the set $\mathscr{X}$ and that there is no intersection between the P_i-s.

Definition 2. *Given a partition $\{P_i^{\mathrm{N}}\}_{i=1}^k$ of a compact set $\mathscr{X} \subseteq \mathbb{R}^2$, let $N_i = \{j = N^+ \mid \partial P_i^{\mathrm{N}} \cap \partial P_j^{\mathrm{N}} \neq \emptyset, i \neq j\}$. Then, $\{P_i^{\mathrm{N}}\}_{i=1}^k$ is called an 2-neighbor partition if $|N_i| \leq 2 \; \forall i \neq j$.*

Here $|S|$ denotes the number of element of the set S and ∂S denotes the boundary of the set S. The superscript "N" stands for neighbor. The definition means that the P_i^{N}-s cover the set $\mathscr{X}$ and that each P_i^{N} has at most two neighbours; see Fig. 4(b).

Definition 3. *Given a partition $\{P_i\}_{i=1}^k$, an ε-partition of a compact set $\mathscr{X} \in \mathbb{R}^2$ is a collection of subsets $\{P_i^\varepsilon\}_{i=1}^k$, $P_i^\varepsilon \subseteq \mathscr{X}, P_i^\varepsilon \neq \emptyset$, such that $\bigcup_{i=1}^k P_i^\varepsilon = \mathscr{X}$ and $P_i^\varepsilon \setminus P_j^\varepsilon \neq \emptyset, \forall i \neq j$, where $\varepsilon = \inf\{\rho > 0 \,|\, P_i^\varepsilon \subseteq (P_i \bigoplus B_\rho) \cap \mathscr{X}, \forall i\}$.*

Here, B_ρ denotes a ball with radius ρ around the origin and $\bigoplus$ denotes the Minkowski sum defined by $A \bigoplus B = \{z = x + y | x \in A, y \in B\}$. This definition means that the P_i^ε-s cover the set $\mathscr{X}$ and that each P_i^ε intersects with its neighbours, while ε is the smallest radius for the ball that allows us to cover the intersecting regions; see Fig. 4(c). It is clear that as $\varepsilon \to 0$, an ε-partition $\{P_i^\varepsilon\}_{i=1}^k$ converges to a partition $\{P_i\}_{i=1}^k$.

Definition 4. *A 2-neighbor ε-partition of a compact set $\mathscr{X}$ is an ε-partition $\{P_i^{\mathrm{N}\varepsilon}\}_{i=1}^k$ of that set such that $|N_i| \leq 2, \forall i$ and $Q_{i,j}^{\mathrm{N}\varepsilon} \bigcap Q_{i,l}^{\mathrm{N}\varepsilon} = \emptyset, \; \forall j,l \in N_i$ where $N_i = \{j \in \mathbb{N}^+ | P_i^{\mathrm{N}\varepsilon} \bigcap P_j^{\mathrm{N}\varepsilon} \neq \emptyset, i \neq j\}$ and $Q_{i,j}^{\mathrm{N}\varepsilon} = P_i^{\mathrm{N}\varepsilon} \bigcap P_j^{\mathrm{N}\varepsilon}$.*

This definition means that the $P_i^{\mathrm{N}\varepsilon}$-s cover the set $\mathscr{X}$ and each $P_i^{\mathrm{N}\varepsilon}$ intersects with its neighbors but there will be at most two neighbors for each $P_i^{\mathrm{N}\varepsilon}$; see Fig. 4(d).

Lemma 3. *Given a 2-neighbor ε-partition of a set $\mathscr{X}$, $\{P_i^{\mathrm{N}\varepsilon} \backslash (\bigcup_{j \in N_i} Q_{i,j}^{\mathrm{N}\varepsilon})\}_{i=1}^k \bigcup \{\bigcup_{j \in N_i} Q_{i,j}^{\mathrm{N}\varepsilon}\}_{i=1}^k$ gives a partition of the set $\mathscr{X}$.*

Proof. This is trivial since there is no intersection between any two intersections of any two of the partition elements $Q_{i,j}^{\mathrm{N}\varepsilon} = P_i^{\mathrm{N}\varepsilon} \bigcap P_j^{\mathrm{N}\varepsilon}$. □

Lemma 4. *A full-rank affine transformation preserves partition (or ε-partition or 2-neighbor partition or 2-neighbor ε-partition) of a set $\mathscr{X} \subseteq \mathbb{R}^2$.*

Proof. We prove this by contradiction. Suppose that the image of a partition is not a partition any more. It could be that $\bigcup_{i=1}^k P_i \neq \mathscr{X}$ or $\exists i \neq j$, $P_i \bigcap P_j \neq \emptyset$. Both cases imply that $\exists Q \in \mathrm{Im}(\mathscr{X}), Q \neq \emptyset$ such that $\mathrm{Pre}(Q) = \emptyset$, that is, the affine transformation maps a point to a nonempty set, which cannot be true for a full-rank affine transformation. □

Based on these definitions and lemmas, we give two assumptions that are satisfied by the shift schedule designed in the previous section.

Assumption 1. *The gear shift logic (23) gives a 2-neighbor ε-partition in the (ω_e, T_e) space, and therefore also in the (v, a_d)-space and in the $(\tilde{v}, \tilde{a}_d)$-space. If $\varepsilon = 0$ the gear shift logic gives 2-neighbor partitions in all these spaces.*

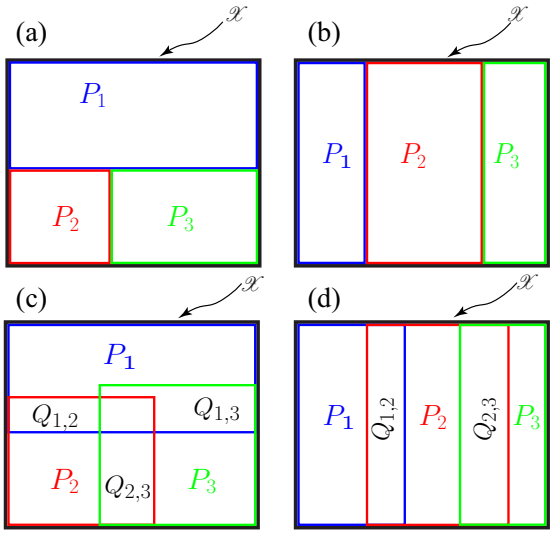

Figure 4: Visualization of definitions (a) Partition (b) 2-neighbor partition (c) ε-partition (d) 2-neighbor ε-partition.

Using the affine transformations (8,12), we can translate the gear shift design proposed (23) from (ω_e, T_e) to (v, a_d). In practice, the BSFC is usually close to a quadratic function with one minimum point, and it can be shown that for a quadratic BSFC function Assumption 1 holds. As will be shown below, such assumption is essential to prove the stability of a gear switch schedule, so one shall generate a 2-neighbor ε-partition in the (v, a_d) plane even when the BSFC is more complicated.

As mentioned above, due the introduction of engine saturation, the stability of a trivial equilibrium may not be guaranteed in theory. With the transformation (12) between (ω_e, T_e) and (v, a_d), the constraints (16) become

$$v \in [0, \bar{v}], \quad a_d \in [\underline{a}_d, \bar{a}_d], \quad m_{\text{eff}} a_d v < P_{\max}, \tag{24}$$

where we also assumed that, by applying the brake, the velocity can be reduced to zero and the minimum control $\underline{a}_d$ can be smaller than suggested by the minimum engine torque $\underline{C}(\omega_e)$. For simplicity, we set $\underline{a}_d, \bar{a}_d$ independent of v. Based on these constraints, we also make the following assumption.

Assumption 2. *The trivial equilibrium of the dynamic system* (9) *with the PI controller* (4) *is still asymptotically stable and the set* (24) *is invariant if* $\tilde{v} > -K_P/k - 2v^*$.

Using Lemma 4, we can conclude that if the shift logic boundary (23) gives a 2 neighbor ε-partition, it maps all equilibria of the model (6) that are not located in an intersecting region of the ε-partition to a unique equilibrium of the switched system (14). Recall that in Lemma 1, we used the $(\tilde{v}, \tilde{a}_d)$ space and we follow this convention in the next theorem.

Theorem 1. *If Assumptions 1 and 2 hold, the gear change will settle down after finitely many switches.*

Proof. Denote working region of engine in $(\tilde{v}, \tilde{a}_d)$-space as $\mathscr{X}$, and 2-neighbor ε-partition generated by gear change as $\bigcup_{i=1}^{N} P^{N\varepsilon}$. We define $Q_{i,j}^{N\varepsilon} = P_i^{N\varepsilon} \bigcap P_j^{N\varepsilon}$. The initial states are $(\tilde{v}_0, \tilde{a}_{d0})$ at $t = 0$. According to Assumption 2, the equilibrium of (9) is asymptotically stable. Define the domain $D_\delta = \{(\tilde{v}, \tilde{a}_d) | V(\tilde{v}, \tilde{a}_d) \le \delta\}$, where V is the Lyapunov function (10). Below we use the abbreviated notation $D_{V(\tilde{v}_0, \tilde{a}_{d0})}$, by which we mean D_δ with $\delta = V(\tilde{v}_0, \tilde{a}_{d0})$. Without loss of generality, we assume that the equilibrium (v^*, a_d^*) is located in $P_i^{N\varepsilon}$, while the initial state $(\tilde{v}_0, \tilde{a}_{d0})$ can be in any gear. Then there are three possibilities.

1. The equilibrium is located in a non-intersecting region (i.e., $(v^*, a_d^*) \notin Q_{i,j}^{N\varepsilon}, \forall j \neq i$), and the initial state $(\tilde{v}_0, \tilde{a}_{d0}) \in D_{V(\tilde{v}_0, \tilde{a}_{d0})} \subseteq P_i^{N\varepsilon}$. If $(\tilde{v}_0, \tilde{a}_{d0}) \in P_i^{N\varepsilon} \bigcap P_j^{N\varepsilon}$ where $j \in N_i$, and the system start in the j-th gear, then one gear change will happen and the trajectory settles to the i-th gear, yielding a stable equilibrium. If, instead, the system starts in the i-th gear, then no gear change will happen while the trajectory approaches the equilibrium.
2. The equilibrium is located in an non-intersecting region, but the trajectory of $(\tilde{v}, \tilde{a}_d)$ may travel through different regions, that is $D_{V(\tilde{v}_0, \tilde{a}_{d0})} \bigcap P_j^{N\varepsilon} \backslash Q_{i,j}^{N\varepsilon} \neq \emptyset, \exists j \neq i$. In this case multiple gear shifts may occur. By Assumption 1 there is a non-zero dwell time between two consecutive gear shifts. Then $\exists T > 0$ such that $\forall t > T$, $D_{V(\tilde{v}(t), \tilde{a}_d(t))} \subseteq P_i^{N\varepsilon}$. Since T is finite, it will enter and leave $P_j^{N\varepsilon}, \forall j \neq i$ only finite times. Therefore the gear will still settle down to the i-th gear and the equilibrium will be stable.
3. The equilibrium is located in an intersecting region, i.e., $\exists j \in N_i$ such that $(v^*, a_d^*) \in Q_{i,j}^{N\varepsilon}$. If $D_{V(\tilde{v}_0, \tilde{a}_{d0})} \subset Q_{i,j}^{N\varepsilon}$, the states converge to the equilibrium without changing gears and the equilibrium is stable (the final gear could be either i or j). If $D_{V(\tilde{v}_0, \tilde{a}_{d0})} \not\subset Q_{i,j}^{N\varepsilon}$, then $\exists T > 0$ such that $\forall t > T$, $D_{V(\tilde{v}(t), \tilde{a}_d(t))} \subseteq Q_{i,j}^{N\varepsilon}$. Since T is finite, the trajectory will enter and leave $P_j^{N\varepsilon}, (j \neq i)$ only finite times. Therefore the gear will still settle down at the same gear as $\big(\tilde{v}(T), \tilde{a}_d(T)\big)$ (also could be either i or j).

All the scenarios are illustrated in Fig. 5, where initial conditions are denoted by black crosses while equilibria are denoted by blue

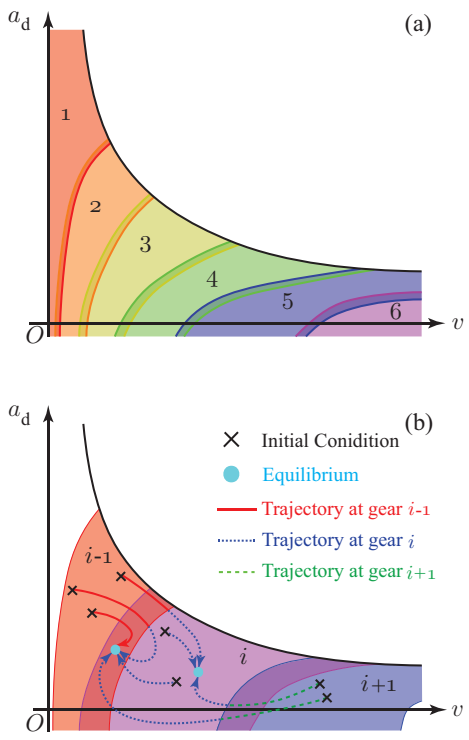

Figure 5: (a) 2-neighbor ε-partition generated by switching logic and (b) zoomed version with trajectories shown

dots. □

Based on the proof above, we can guarantee that our gear shift logic forces the system to converge to the equilibrium. With Lemma 4, the logic also stabilizes the dynamic model with gear change (14) in the extended state space (ω_e, T_e, i), as long as Assumptions 1 and 2 holds. We remark that Assumption 2 can be generalized to allow a stabilizing controller $u(\tilde{v}, \tilde{a}_d)$ of non-PI type.

5 CASE STUDY

In this section we test the gear shift logic using different driving cycle data for a class 8 Prostar truck manufactured by Navistar company that is equipped with a MaxxForce 13 liter diesel engine and with a 10 speed automated manual transmission. The parameters for the vehicle are given in Appendix A. The gear ratios η_i are given by the corresponding value in the table times the final drive ratio. During the simulations, the efficiency for torque delivery among gears is also considered. The feedback parameters are set to $K_I = 1[1/s^2]$ and $K_P = 6[1/s]$.

We compare the proposed method with a standard gear shift design widely used in industry [3]. Our design is shown in Fig. 6(a) that gives a 2-neighbor ε-partition over (v, a_d) space and we use $\varepsilon = 0.05$. The standard design is shown in Fig. 6(b) that also gives a 2-neighbor ε-partition (but ε is not known here a priori). The fuel consumptions are calculated for two different EPA driving cycles [20], namely, the heavy duty urban dynamometer driving schedule (HDUDS) cycle and the New York City (NYC) cycle. In both cases we rescaled the speed to make sure that the gear selection logic can accommodate torque demand for a fully loaded class 8 truck. The resulting driving profiles are shown in Fig. 7. It can be see that the two designs result in identical speed profiles, but the engine is at different working conditions.

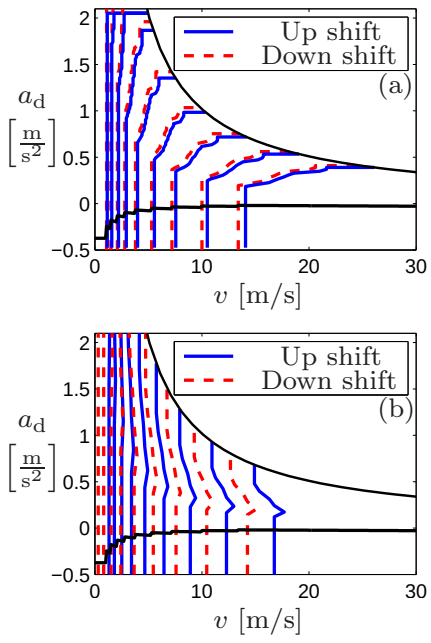

Figure 6: Gear change map in (v, a_d) space resulted from (a) the presented optimal design and from (b) the benchmark design in [3].

Driving Cycle	HDUDS	NYC
Benchmark Design (MPG)	6.42	3.56
Optimal Design (MPG)	6.57	3.65
Theoretical Upper Bound (MPG)	6.62	3.68

Table 1: Fuel consumption results

The fuel consumption results are summarized in Table 1. The optimal design refers to the shift logic using the presented method, while the benchmark design refers to the standard approach. The theoretical upper bound refers to the optimal design with $\varepsilon = 0$ where gear skipping is also allowed. Therefore the theoretical upper bound is not possible to achieve in practice, but it does provide the upper bound of the fuel economy for a given driving cycle. It can be seen that for both driving cycles, our design manages to improve fuel economy, by pushing it closer to the theoretically limit while delivering the required torque.

One may notice in Fig. 7(b,d) that the gear change of the optimal design is relatively frequent compared to the standard design. This is because the optimal shift logic depends on data given by the engine BSFC map, so the resulted gear shift curves $H_{i\varepsilon}^+$ and $H_{i\varepsilon}^-$ may be of zig-zag shaped. Also, the choice of the parameter ε effects the gear shift. Having a small ε makes a gear shift logic perform closer to theoretical upper bound, but tends to generate more frequent gear changes. By contrast, having a large ε leads to less frequent gear changes but compromises fuel economy. Therefore, the value ε requires fine tuning in the practical design for specific engines. Nonetheless, the principle for choosing the gear shift logic is the right approach if the main design objective is to improve fuel economy. To further improve the fuel economy, one may focus on regulating the driving profile of while adapting to the dynamic traffic environment [21].

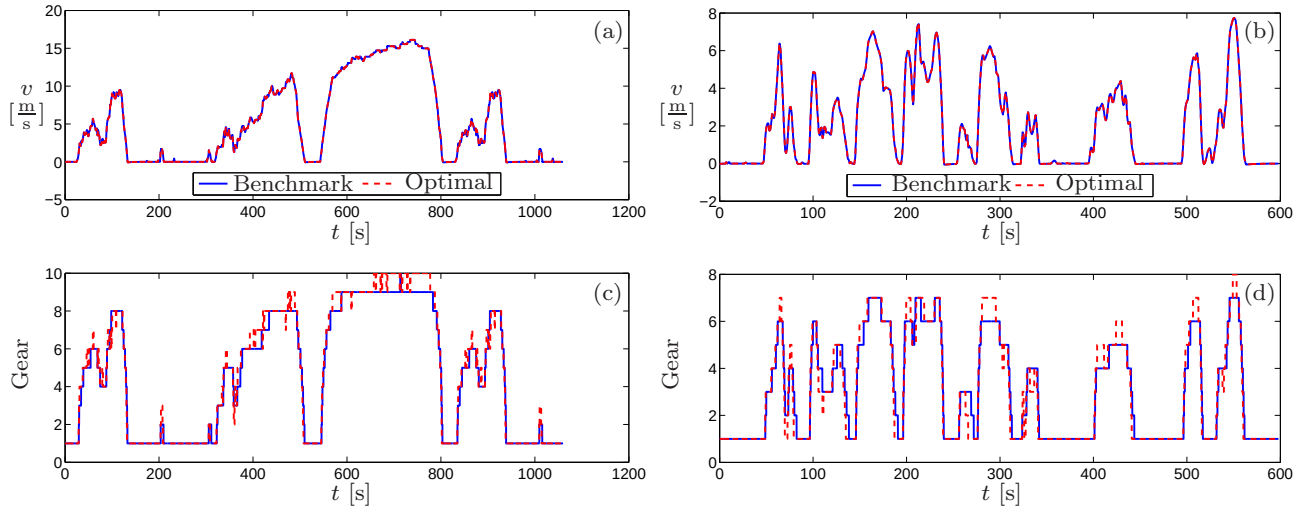

Figure 7: Speed profile and gear change profile for (a) EPA HUDDS driving cycle (b) EPA NYC driving cycle

6 CONCLUSION

In this paper, we proposed an optimizations-based strategy for gear scheduling that could be applied to both human-driven and semi-autonomous vehicles. We used Lyapunov arguments to prove stability of working points in the underlying hybrid dynamic systems. We demonstrated through a case study that our gear shifting strategy outperforms the traditional method. Future works include designing systematic methods to prevent frequent gear changes as well as an investigation on how to fine tune the design parameters in systematic way.

ACKNOWLEDGEMENT

The authors would like to thank the NAVISTAR company for providing the source data used in this paper.

REFERENCES

[1] Kim, D., Peng, H., Bai, S., and Maguire, J. M., 2007. "Control of integrated powertrain with electronic throttle and automatic transmission". *IEEE Transactions on Control Systems Technology,* ***15***(3), pp. 474–482.

[2] Ngo, V. D., Navarrete, J. A. C., Hofman, T., Steinbuch, M., and Serrarens, A. "Optimal gear shift strategies for fuel economy and driveability". *Proceedings of the Institution of Mechanical Engineers, Part D,* ***277***, pp. 1398–1413.

[3] Bai, S., Maguire, J., and Peng, H., 2013. *Dynamic Analysis and Control System Design of Automatic Transmissions*. SAE International.

[4] Tan, J., Yin, X., Lei, Y., and Ge, A., 2005. "Research on a neural network model based automatic shift schedule with dynamic 3-parameters". In SAE Technical Paper, SAE International.

[5] Qin, G., Ge, A., and Lee, J.-J., 2004. "Knowledge-based gear-position decision". *IEEE Transactions on Intelligent Transportation Systems,* ***5***(2), pp. 121–125.

[6] Li, G., and Hu, J., 2010. "Modeling and analysis of shift schedule for automatic transmission vehicle based on fuzzy neural network". In 8th World Congress on Intelligent Control and Automation (WCICA), IEEE, pp. 4839–4844.

[7] Liu, Y., Qin, D., Jiang, H., Liu, C., Zhang, Y., and Lei, Z., 2009. "Shift schedule optimization for dual clutch transmissions". In Vehicle Power and Propulsion Conference, IEEE, pp. 1071–1078.

[8] Liu, Y. G., Qin, D. T., Lei, Z. Z., and Ding, R., 2011. "Intelligent correction of shift schedule for dual clutch transmissions based on different driving conditions". *Applied Mechanics and Materials,* ***121-126***, pp. 3982–3987.

[9] Ge, J. I., and Orosz, G., 2014. "Dynamics of connected vehicle systems with delayed acceleration feedback". *Transportation Research Part C, Emerging Technologies,* ***46***, pp. 46–64.

[10] Lin, H., and Antsaklis, P. J., 2009. "Stability and stabilizability of switched linear systems: a survey of recent results". *IEEE Transactions on Automatic control,* ***54***(2), pp. 308–322.

[11] Branicky, M. S., 1998. "Multiple Lyapunov functions and other analysis tools for switched and hybrid systems". *IEEE Transactions on Automatic Control,* ***43***(4), pp. 475–482.

[12] Bernardo, M., Budd, C., Champneys, A. R., and Kowalczyk, P., 2008. *Piecewise-smooth dynamical systems: theory and applications*, Vol. 163 of *Applied Mathematical Sciences*.

[13] Ahmadi, M., Mojallali, H., and Wisniewski, R., 2014. "Guaranteed cost H_∞ controller synthesis for switched systems defined on semi-algebraic sets". *Nonlinear Analysis: Hybrid Systems,* ***11***, pp. 37–56.

[14] Liu, J., Liu, X., and Xie, W.-C., 2010. "On the (h_0, h)-stabilization of switched nonlinear systems viastate-dependent switching rule". *Applied Mathematics and Computation,* ***217***(5), pp. 2067–2083.

[15] Jin, Y., Fu, J., Zhang, Y., and Jing, Y., 2014. "Reliable control of a class of switched cascade nonlinear systems with its application to flight control". *Nonlinear Analysis: Hybrid Systems,* ***11***, pp. 11–21.

[16] Liu, J., Ozay, N., Topcu, U., and Murray, R. M., 2013. "Synthesis of reactive switching protocols from temporal logic specifications". *IEEE Transactions on Automatic Control,* ***58***(7), pp. 1771–1785.

[17] Orosz, G., and Shah, S. P., 2012. "A nonlinear modeling framework for autonomous cruise control". In Proceedings of ASME Dynamic Systems and Control Conference, no. DSCC2012-MOVIC2012-8871, ASME, pp. 467–471.

[18] Alam, A., 2014. "Fuel-efficient heavy duty vehicle platooning". PhD thesis, Kungliga Tekniska Högskolan.

[19] Heywood, J. B., 2002. *Internal combustion engine fundamentals*. McGraw-Hill.

[20] US EPA dynamometer driving schedules. `http://www.epa.gov/oms/emisslab/testing/dynamometer.htm`.

[21] He, C. R., and Orosz, G., 2014. "Fuel consumption optimization of heavy-duty vehicles: An analytical approach". In Proceedings of the ASME Dynamic Systems and Control Conference, no. DSCC2014-6362, p. V002T20A006.

[22] Navistar, 2011. Maxxforce 11 and 13 liter engines. Tech. rep., Navistar Inc.

A TABLE OF PARAMETER OF NAVISTAR TRUCK

Parameter	Value
Mass (m)	29484 [kg]
Air Drag Coefficient (k)	3.84 [kg/m]
Tire Rolling Radius (R)	0.504 [m]
Tire Rolling Resistance Coefficient (γ)	0.006
Maximum Acceleration ($a_{\max}$)	2 $[\mathrm{m/s^2}]$
Engine Rotational Inertia (I)	39.9 $[\mathrm{kg{\cdot}m^2}]$
Gravitational Constant (g)	9.81 $[\mathrm{m/s^2}]$
Number of Forward Gears	10
1st Gear Ratio/Efficiency	12.94/0.97
2nd Gear Ratio/Efficiency	9.29/0.97
3rd Gear Ratio/Efficiency	6.75/0.97
4th Gear Ratio/Efficiency	4.9/0.97
5th Gear Ratio/Efficiency	3.62/0.97
6th Gear Ratio/Efficiency	2.64/0.97
7nd Gear Ratio/Efficiency	1.90/0.97
8rd Gear Ratio/Efficiency	1.38/0.98
9th Gear Ratio/Efficiency	1/0.99
10th Gear Ratio/Efficiency	0.74/0.98
Final Drive Ratio /Efficiency	4.17/0.98

Table 2: Data of a 2012 Navistar Prostar truck [22].